NANO · MICRO small
www.small-journal.com

Water-Induced Separation of Polymers from High Nanoparticle-Content Nanocomposite Films

*Baekmin Q. Kim, Máté Füredi, R. Bharath Venkatesh, Stefan Guldin, and Daeyeon Lee**

Polymer nanocomposites with high loadings of nanoparticles (NPs) exhibit exceptional mechanical and transport properties. Separation of polymers and NPs from such nanocomposites is a critical step in enabling the recycling of these components and reducing the potential environmental hazards that can be caused by the accumulation of nanocomposite wastes in landfills. However, the separation typically requires the use of organic solvents or energy-intensive processes. Using polydimethylsiloxane (PDMS)-infiltrated SiO_2 NP films, we demonstrate that the polymers can be separated from the SiO_2 NP packings when these nanocomposites are exposed to high humidity and water. The findings indicate that the charge state of the NPs plays a significant role in the propensity of water to undergo capillary condensation within the PDMS-filled interstitial pores. We also show that the size of NPs has a crucial impact on the kinetics and extent of PDMS expulsion, illustrating the importance of capillary forces in inducing PDMS expulsion. We demonstrate that the separated polymer can be collected and reused to produce a new nanocomposite film. The work provides insightful guidelines on how to design and fabricate end-of-life recyclable high-performance nanocomposites.

1. Introduction

Polymer nanocomposite films and membranes with extremely high loadings of nanoparticles (NPs) above ≈50 vol.% are highly desirable for a range of applications including protective coatings,[1–5] separation membranes,[6,7] optical films,[8,9] displays,[10] sensors[11,12] and energy devices[13,14] due to their exceptional mechanical and transport properties. Natural nanocomposites, such as nacre and tooth enamel, are known for their ultrahigh toughness and strength, which are achieved through high concentrations of hard NPs as well as the intricate nano/micro-scale structure of these composites.[1–5] Recent research has shown that it is possible to emulate the structure of these natural composites, resulting in nanocomposite films with high strength and toughness ideal for protective and structural applications.[1–5,15–18] Highly loaded nanocomposite films also exhibit excellent thermal and electrical conductivities due to the percolation of NPs, when thermally and electrically conductive NPs are used.[19–22] Various strategies have been developed to produce highly loaded nanocomposite films, coatings, and membranes, such as layer-by-layer processes,[3,4] polymerizing monomers in the interstitial pores of pre-assembled NP packings,[13,20,22,23] inducing infiltration of polymers into the voids of NP packings by capillary rise infiltration (CaRI)[9,16–20,24–26] or solvent-driven infiltration of polymer (SIP).[19,27]

To enable widespread utilization of these nanocomposites with extremely high loadings of NPs, it will become increasingly important to develop strategies for recycling these composites, which inevitably will require the separation and reclamation of NPs and polymers. Currently, very few methods of efficiently separating NPs and polymers in nanocomposites without using high-energy methods and harsh organic solvents exist.[28,29] Because of the challenges associated with separating polymers and NPs, nanocomposite wastes typically end up in landfills or are incinerated which leads to NPs entering the waste streams and potentially posing environmental hazards.[30–32] Designing and fabricating end-of-life recyclable nanocomposites will become increasingly important. Besides working toward a sustainable use of highly loaded nanocomposites, separating, and removing unwanted polymeric contaminants from porous materials like NP packings is critical in maintaining the functionality and performance of the NP assemblies, which themselves have useful functionality.

In this study, we demonstrate that polymers can be spontaneously separated and recovered from nanocomposite films with high loadings of NPs with the aid of water from the vapor or the liquid phases. We use polydimethylsiloxane (PDMS)-infiltrated SiO_2 NP films as a model system because of the low glass transition temperature of PDMS and the high concentration of SiO_2 in the nanocomposite (≈64 vol.%). The separation of PDMS from disordered SiO_2 NP packings depends strongly on the charge state of the SiO_2 NPs. Under high humidity and water, PDMS stays within the interstitial voids of ionized SiO_2 NP packings, whereas PDMS is expelled from the packings of unionized SiO_2

B. Q. Kim, R. B. Venkatesh, D. Lee
Department of Chemical and Biomolecular Engineering
University of Pennsylvania
Philadelphia, PA 19104, USA
E-mail: daeyeon@seas.upenn.edu
M. Füredi, S. Guldin
Department of Chemical Engineering
University College London
London WC1E 7JE, UK

The ORCID identification number(s) for the author(s) of this article can be found under https://doi.org/10.1002/smll.202302676

DOI: 10.1002/smll.202302676

Table 1. Specifications of the SiO_2 NP aqueous dispersions[a].

Name	Size [nm]	Concentration [wt%]	Counterion	pH
SM-30	7	30	Na^+	10.0
TM-50	22	50	Na^+	9.0
ST-YL	60	40	Na^+	9.0-10.0

[a] All are provided by the vendors.

NPs by infiltrated water. We rationalize such dependence on the SiO_2 NP surface chemistry based on the kinetics of nucleation for capillary condensation.[33–35] The expulsion of PDMS is also strongly influenced by the relative humidity (RH) as well as the size of NPs, showcasing the role of capillarity in inducing polymer expulsion. The polymer expelled from the nanocomposite can be collected using an elastomer and reused for the fabrication of nanocomposites. The method described in this study to induce the separation of polymers and NPs from highly loaded nanocomposite films does not require any organic solvents and can be performed without relying on a highly energy-intensive process. The ability to separate and recover polymers from packings of NPs also has deep implications for the decontamination of porous membranes, soil, and earth.

2. Results and Discussion

We use polymer-infiltrated NP films (PINFs) to test our hypothesis that water can induce the separation of polymer and NPs in highly loaded nanocomposites. PINFs have emerged as a versatile class of nanocomposites with exceptional mechanical and transport properties owing to the high concentrations of NPs (>64 vol%), large polymer-NP interfacial area, and extreme nanoconfinement of polymers.[9,16–20,24–27] PINFs for this study are prepared by infiltrating a hydrophobic polymer, PDMS into the interstices of dense disordered packings of hydrophilic SiO_2 NPs. PDMS has a low glass transition temperature (<−100 °C),[36] thus its fate can be observed at room temperature. When a PDMS solution is spin-coated onto a SiO_2 NP film, a bilayer film consisting of a PDMS overlayer and a SiO_2 NP packing partially filled with PDMS is initially formed; this bilayer film then spontaneously evolves into a PDMS-infiltrated SiO_2 NP film as the PDMS layer atop the SiO_2 NP packing infiltrates into the interstitial voids of the NP packing via capillary rise infiltration (CaRI);[9,16–20,24–26] when the void volume of the NP packing and the volume of dry PDMS are the same, a PINF with no residual PDMS overlayer is prepared. We fabricate such PINFs with thicknesses of ≈250 nm (Figure S1, Supporting Information) to study the fate of PDMS under high humidity or liquid water. The specifications of the SiO_2 NP aqueous dispersions used to prepare the SiO_2 NP films are given in **Table 1**. The refractive index of a bare SiO_2 NP film at the wavelength of 632.8 nm is 1.302. The refractive index of the film increases to 1.437 upon the infiltration of PDMS into the NP interstitial voids, and its color changes as shown in **Figure 1**a. This refractive index value is slightly smaller than the theoretically estimated value based on the sum of the refractive indices per volume of the constituents (1.440), likely because a small volume of water exists within the film due to capillary condensation (<10 vol.%).[8,26,27]

When an as-prepared PDMS-infiltrated 22 nm SiO_2 NP film is exposed to high humidity (RH ≈95%) or liquid water, no apparent changes in the macroscopic appearance of the film are observed, and the refractive index of the film, as determined by ellipsometry, remains constant. Serendipitously, we find that if PDMS is infiltrated into a SiO_2 NP film after the film was rinsed with deionized (DI) water and subsequently this PDMS-infiltrated SiO_2 NP film is exposed to high humidity, the color of the film changes dramatically from orange to purple as shown in Figure 1a. We focus on the analysis of these films that are prepared by rinsing the SiO_2 NP film with DI water prior to PDMS infiltration. When such a PINF is submerged in liquid water for 10 s and then taken out, the refractive index of the film decreases to 1.334, indicating approximately 85% of PDMS has been removed. By placing a water-sessile drop on top of the PINF and observing this area under a microscope (Figure S2, Supporting Information), PDMS droplets are seen to emerge and rise from the surface (Figure 1a). After the expulsion of PDMS, the color of the area where the water sessile drop was placed returns to that of the bare SiO_2 NP films (Figure 1a), as seen in Figure S2 (Supporting Information). We also observe that PDMS is expelled from SiO_2 NP packings under the high humidity condition if the packings are prepared using SiO_2 NP dispersions that were dialyzed against DI water. Likewise, when PDMS is infiltrated into a SiO_2 NP packing that was rinsed with DI water and then rinsed again with NaOH solution (pH 10), exposure of such a film does not induce any change in the appearance of the film under the high humidity condition.

The color change exhibited by the PINF upon exposure to high humidity as shown in Figure 1a likely indicates a major change in the structure of the film. To gain a better insight into the structural change, spectroscopic ellipsometry is carried out using a two-layer Cauchy model; attempts to use other types of multi-layer Cauchy model lead to poor modeling. As presented in **Figure 2**b, a new layer with a refractive index equal to that of PDMS is indeed formed on top as soon as the film is exposed to high humidity. At the same time, the refractive index of the NP layer (the underlayer) decreases, implying a loss of PDMS. However, the refractive index of the NP layer suggests the presence of water in the interstitial voids (≈50 vol.% of the voids). All these changes indicate that a bilayer consisting of a pure PDMS layer atop the NP layer is formed due to the expulsion of PDMS from the NP layer.

We believe that the driving force for the PDMS expulsion under high humidity is the capillary condensation of water vapor within the NP interstitial voids of the NP packing. Typically, capillary condensation occurs when the interface between the condensate liquid-vapor phase can be stabilized at vapor pressure below the saturation pressure of the molecule due to the high negative curvature of the interface.[8,26,27] Analogous to capillary condensation, we believe that water vapor is undergoing capillary condensation in the PDMS-filled NP packing. Because the SiO_2 surface favors water over PDMS (Figure S4, Supporting Information)[37] and PDMS has a high water permeability,[38,39] water is able to undergo capillary condensation and displace PDMS from the NP packing as depicted in Figure 2a. We believe that the nucleation of capillary bridges occurs at the contacts between SiO_2 NPs and the growth of these bridges pushes the PDMS out of the pores. As water vapor does under high humidity, water from the bulk phase can permeate through the PDMS to induce nu-

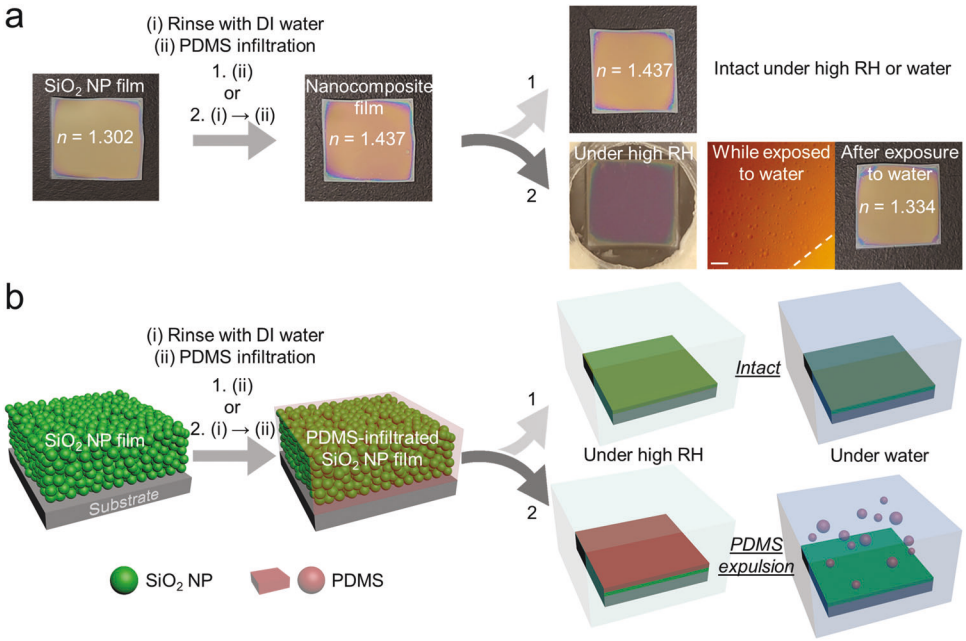

Figure 1. a) Actual appearance of the representative PDMS-infiltrated 22 nm-SiO_2 NP films under high humidity or liquid water depending on whether the base SiO_2 NP films are rinsed with DI water, and b) their schematic illustrations. *n* indicates refractive index of a film at the wavelength of 632.8 nm. The area above the white dashed line indicates where a water-sessile drop is placed. The scale bar is 100 μm.

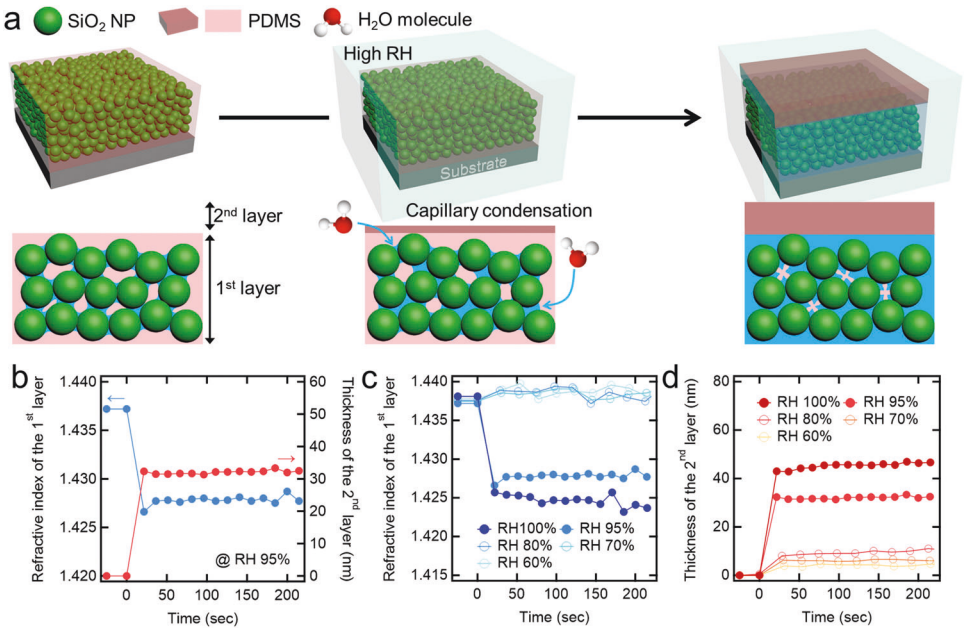

Figure 2. a) Schematic illustration of the mechanism by which PDMS is expelled from a PDMS-infiltrated SiO_2 NP film prepared from a DI water-rinsed SiO_2 NP film under high humidity, and b–d) actual changes in the refractive index of the NP underlayer (1st layer) and the thickness of the expelled PDMS layer (2nd layer) according to the PDMS expulsion from the PDMS-infiltrated 22 nm-SiO_2 NP film prepared from a DI water-rinsed SiO_2 NP film under various humidity conditions. The humidity starts to rise at time = 0 s and reaches the target RH before the first data point is taken.

cleation and growth of capillary bridges in the interstitial voids of the PDMS-filled NP packing because of the high affinity of the SiO_2 NP surface for water over PDMS (Figure S4, Supporting Information).[37] We do not believe the PDMS is displaced by water due to gravitational or buoyancy-driven mechanisms since the Bond number (*Bo*) of the system, which represents the ratio of the gravitational force to interfacial tension force,[40] is far below 1 due to the nanoscale interstitial voids. However, we cannot completely rule out the possibility of the capillarity-induced wicking of water into the PDMS-filled pores displacing PDMS akin to the

wicking of water into air-filled pores.[41–43] We also confirm that PDMS introduced into the nanopores of the NP packing without using solvent[26] also undergoes expulsion from the nanopores upon exposure to high humidity or water, indicating that this behavior does not depend on the presence of a residual solvent.

The thickness of the expelled PDMS layer and the refractive index of the NP underlayer reach ≈30 nm and 1.428, respectively. The amount of PDMS that is expelled from the NP packing is consistent with the amount expected from the refractive index reduction in the NP underlayer, which now consists of water, SiO_2 NPs, and residual PDMS. The reduction in the refractive index of the NP underlayer and the increase in the thickness of the expelled PDMS layer increases with RH, as shown in Figure 2c,d. These results support that the expulsion of PDMS is driven by the capillary condensation of water vapor in the PDMS-filled NP packing.

We now turn our attention back to the two different types of SiO_2 NP films that showed vastly different behavior when exposed to high humidity or liquid water. The tendency of the polymer to undergo expulsion depends on whether the bare SiO_2 NP film is rinsed with DI water or not before the PDMS infiltration; such difference points to the fact that the interactions between PDMS and the SiO_2 NP surface are altered due to the charge state of the SiO_2 NP surface. Since the isoelectric point of SiO_2 surfaces is ≈3,[44] SiO_2 NPs are negatively charged and the charge is balanced by cationic counterions (M^+s) in water at the solution pH of 9–10 (the condition used in this study). Prior studies have classified the surface of SiO_2 into three types: Q^2, Q^3, and Q^4 based on the areal density of SiOH groups; the surface of the NPs used in this study has been previously categorized as Q^3, possessing ≈4.7 SiOH groups per nm^2.[45,46] About 20% of the SiOH groups on the surfaces of Q^3 are known to deprotonate and form SiO^--M^+ groups in water at a pH of 9–10.[46,47] The SiO_2 NP films prepared by spin coating the dispersions with Na^+ counterions, thus would have a large number of SiO^-Na^+ surface groups (**Figure 3**a). In contrast, when such a film is rinsed with DI water which has a pH of 5.5–6.0, a large number of the SiO^-Na^+ groups become protonated to form SiOH groups (Figure 3a). This change in the surface chemistry is verified by characterizing the NP surface using energy-dispersive X-ray spectroscopy (EDS). As shown in Figure 3b, the peaks that represent O and Si remain identical in the two SiO_2 NP films, whereas the peak assigned to Na is only observed in the as-prepared unrinsed SiO_2 NP film (inset of Figure 3b). Similar changes in the surface chemistry are observed for the SiO_2 NP films with different NP sizes studied in this work, as seen in Figure S5a (Supporting Information).

Interestingly, both the ionized and the unionized SiO_2 surfaces have preferential interactions with water over PDMS as determined by contact angle measurements (Figure S4, Supporting Information). Thus, solely based on thermodynamic arguments, PDMS expulsion would be predicted for both cases. However, our experimental results unequivocally show that there is a drastic difference between the two cases. To understand how the change in the surface chemistry of SiO_2 NPs can induce the expulsion of PDMS under high humidity and liquid water, we rely on the kinetics of capillary condensation in solid mesopores filled with liquid media. In our system, the SiO_2 NP surfaces and PDMS constitute the solid and liquid phases, respectively. There exists a critical free energy barrier to induce the nucleation and growth

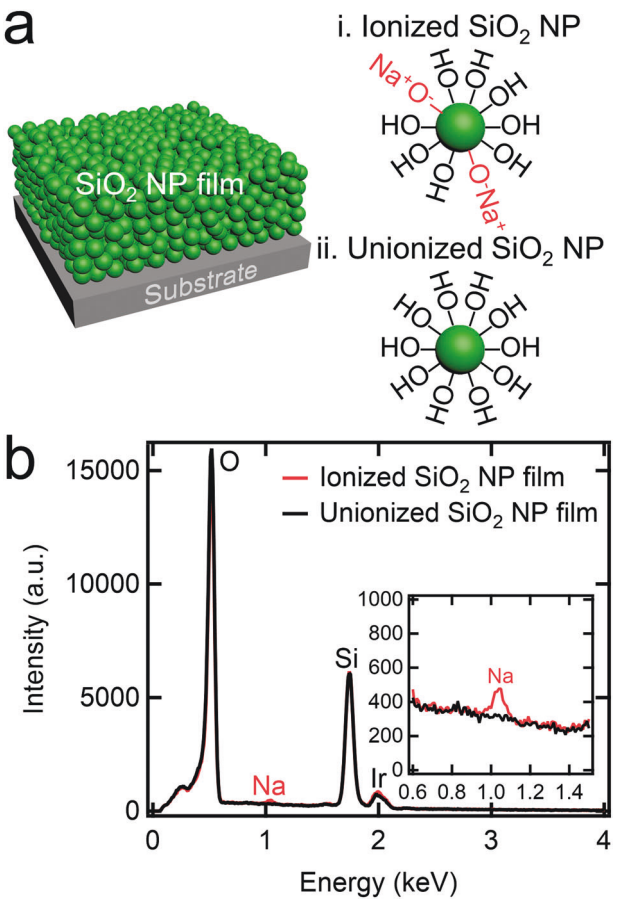

Figure 3. a) Schematic illustration of the ionized and unionized SiO_2 NP films, and b) element characterization of the representative 22 nm-SiO_2 NP films in the two cases using EDS analysis. The peak assigned to Ir is attributed to the metallic coating that is deposited prior to scanning electron microscope observation to prevent charging.

of capillary bridges in nanoscale pores.[33–35] When we estimate the critical free energy barriers for both ionized and unionized 22 nm-SiO_2 NP packings (see Supporting Information for details), the estimated critical free energy barrier for the ionized SiO_2 NP packing is greater by at least ≈30 k_BT (where k_B is the Boltzmann constant and T is temperature) compared to the unionized SiO_2 NP packing. Based on these estimations, we believe that water vapor cannot nucleate in the interstitial pores of the ionized SiO_2 NP packing due to the larger critical free energy barrier, whereas water vapor can nucleate and grow as condensed liquid water in the unionized NP interstitial pores, resulting in the massive expulsion of PDMS. Likewise, liquid water likely experiences a similar energy barrier to nucleate capillary bridges for the ionized SiO_2 NP packing, and thus aqueous bridges are not able to grow and thus PDMS remain intact within the interstitial voids.

The driving force for capillary condensation increases as the NP size decreases due to the increased curvature of the interface.[8,26,27] Consistent with this, the increase in the thickness of the expelled PDMS layer and the reduction in the refractive index of the NP underlayer under high RH is greater with decreasing NP size at a fixed RH, as presented in **Figure 4**a. Moreover, the rate at which PDMS is expelled from the NP packing

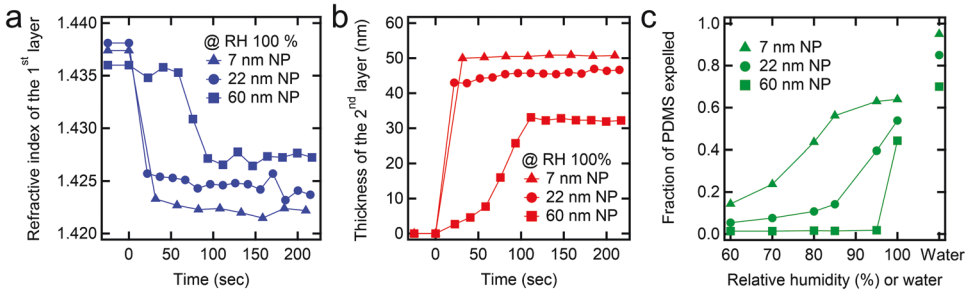

Figure 4. NP size effects on the PDMS expulsion from the PDMS-infiltrated SiO_2 NP films prepared from DI water-rinsed SiO_2 NP films. a) The changes in the refractive index of the SiO_2 NP underlayer (1st layer) at RH 100%. b) The changes in the thickness of the expelled PDMS layer (2nd layer) at RH 100%. c) The changes in the fraction of the PDMS expelled under various humidity conditions and exposure to liquid water.

due to capillary condensation of water vapor becomes faster with decreasing NP size, as shown in Figure 4b, indicating the importance of thermodynamic driving force. Consistent with these observations, when PDMS-infiltrated SiO_2 NP films are submerged under water, as the NP size decreases, a larger volume of water infiltrates, expelling a larger volume of PDMS as shown in Figure 4c. The fraction of PDMS expelled as a function of RH increases with decreasing NP size, as summarized in Figure 4c, indicating that smaller NP size and higher RH are key features that induce PDMS expulsion due to water infiltration.

One of the essential steps that must be implemented to enable the recycling of the separated polymer is its collection. PDMS expelled from the nanocomposite under water can be directly collected using various methods.[48,49] and reused. In contrast, the expelled PDMS layer under high humidity does not spontaneously detach from the NP packing. One way to collect the expelled PDMS under high humidity is to exploit an elastomer that functions as a collection reservoir. A crosslinked PDMS elastomer slab is placed on top of a PDMS-infiltrated SiO_2 NP (unionized) film and is exposed to high RH; the expelled PDMS is absorbed into the elastomer and freed from the NP packing by detaching the elastomer, as shown in **Figure 5**a. In the case of using a PDMS-infiltrated 7 nm-SiO_2 NP film, the refractive index of the film decreases from 1.437 to ≈1.36 at RH ≈100% (Figure 5a), indicating approximately 60% of PDMS has been recovered, consistent with the results in Figure 4c. The PDMS collected in the elastomer can be reused in various ways; for example, when this PDMS-loaded elastomer is placed on top of another SiO_2 NP film, the mobile PDMS chains infiltrate into the interstitial voids,[26] resulting in the formation of a new PINF, as evidenced by the increase of the refractive index of the film from 1.302 to ≈1.44 (Figure 5a).

To demonstrate that the separation of polymer is not limited to a low glass transition temperature polymer such as PDMS but also high glass transition temperature thermoplastics that are used for nanocomposite fabrication can be recovered using the same approach, we test the feasibility of separating polypropylene carbonate (PPC, refractive index = 1.460) which has a glass transition temperature of 35 °C[50] from SiO_2 NP packings. The refractive index of a PPC-infiltrated SiO_2 NP film is 1.454, as shown in Figure 5b. The film is placed in a vial filled with DI water and heated in a water bath at 70 °C for 10 min. The refractive index of the PPC-filled ionized SiO_2 NP packing remains constant, whereas that of the PPC-filled unionized SiO_2 NP packing decreases to 1.336 (Figure 5b), indicating approximately 80% removal of PPC. This extent of expulsion is consistent with the case of PDMS.

3. Conclusion

In this work, we have demonstrated that polymers can be spontaneously separated from PINFs via capillary condensation of water into the interstices of NP packings under high humidity or exposure to liquid water. The separation of PDMS depends strongly on the energy barrier to induce the nucleation and growth of capillary condensation in SiO_2 NP packings that depend on the charge state of NPs as well as the RH and the NP size. The results of this study have implications on the reclamation of non-crosslinked thermoplastic polymers from nanocomposites for recycling as well as the decontamination of porous materials such as NP packings. Moreover, the study provides guidelines for designing end-of-life recyclable nanocomposites with high loadings of NPs. There are several open questions that warrant future studies. The type of counterion, for example, could change the interaction of ionized SiO_2 NP surfaces with water[51] and in turn, affect the extent of polymer expulsion from NP packings. The impact of the NP distribution and the structure of NP packings on the separation of polymer and NPs requires more detailed future investigation. Moreover, the mechanism by which capillary bridges nucleate and grow will benefit substantially from the development of theoretical and computational approaches that account for water density fluctuations in the complex topology of NP packings.[52]

4. Experimental Section

Materials: Monodisperse PDMS (M_n = 15 000 g mol^{-1}, P7273-DMS) and UV-curable PDMS (KER-4690 A and B) are purchased from Polymer Source (Dorval, QC, Canada) and Shin-Etsu Chemical Co., Ltd (Tokyo, Japan), respectively. PPC (M_n ≈50 000 g mol^{-1}, 389021) was purchased from MilliporeSigma (St. Louis, MO, USA). For the SiO_2 NP aqueous dispersions with different NP sizes, Ludox SM-30 and TM-50 are obtained from MilliporeSigma, and Snowtex ST-YL was generously provided by Nissan Chemical America Corp. (Houston, TX, USA). The specifications of the SiO_2 NP aqueous dispersions are given in Table 1. Isopropyl alcohol (Certified ACS Plus), NaOH solution (1 N/Certified), toluene (HPLC Grade), and chloroform (HPLC Grade) were purchased from Fisher Scientific Co LLC (Pittsburgh, PA, USA). Ethanol (200 Proof) was obtained from Decon Laboratories Inc (King of Prussia, PA, USA).

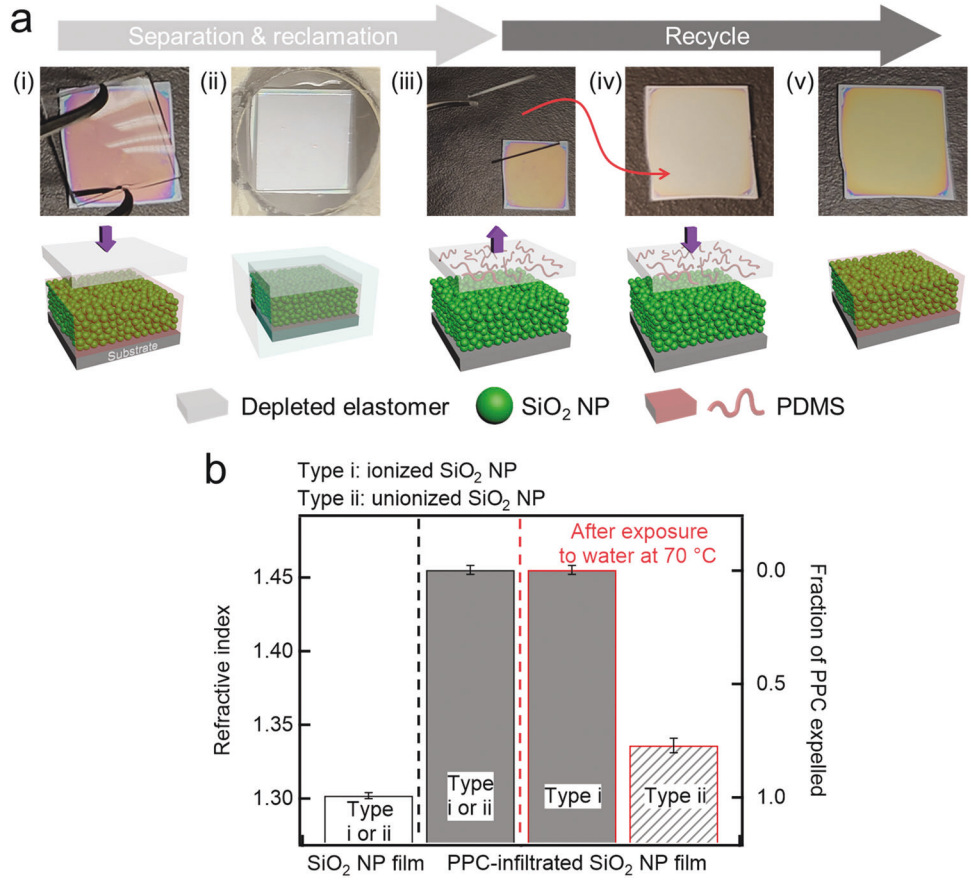

Figure 5. a) Photographic images and schematic illustration of the collection and reuse of the PDMS separated from the PDMS-infiltrated 7 nm-SiO_2 NP (unionized) films under high humidity (RH ≈100%). i) A crosslinked PDMS elastomer slab is placed atop the PINF; ii) the PINF with the elastomer slab on top is exposed to 100% RH; iii) the elastomer slab carrying the expelled PDMS is removed from the PINF; iv) the elastomer slab is placed on top of a newly prepared NP film; v) PDMS from the elastomer slab is infiltrated into the interstices of the NP film and a new PINF is prepared. For the new NP film, a 7 nm-SiO_2 NP (unionized) film with a thickness of ~ 200 nm is used. b) Changes in the refractive index of the PPC-infiltrated 22 nm-SiO_2 NP films prepared from ionized and unionized SiO_2 NP films before and after exposure to heated water. PPC is expelled only from the PPC-infiltrated SiO_2 NP film prepared from the unionized SiO_2 NP film under the heated water.

Preparation of Bare SiO2 NP Films and PINFs: As substrates, Si wafers (452, UniversityWafer, Inc., South Boston, MA, USA) were cleaved into ≈1.5 × 1.5 cm^2 pieces, and the surface of the cleaved wafers were rinsed with isopropyl alcohol and DI water (18.2 MΩ•cm), followed by 5 min of oxygen plasma (PDC-32G, Harrick Plasma Inc., Ithaca, NY, USA) treatment to remove residual organic contaminants. The stock SiO_2 NP aqueous dispersions were diluted with DI water to ≈15 wt%. Some of the diluted dispersions were dialyzed for 120 h against DI water, which was replaced every 24 h, using dialysis tubes (10k MWCO, 68100, Fisher Scientific Co LLC). Prior to use, all the diluted dispersions were sonicated for at least 2 h to ensure homogeneous dispersion of SiO_2 NPs and then filtered using hydrophilic syringe filters with a size cut-off of 0.45 µm (09-720-005, Fisher Scientific Co LLC) to remove NP aggregates. SiO_2 NP films with thicknesses of ≈250 nm were prepared on the Si substrates by spin coating the filtered dispersion using a spin coater (WS-400BZ-6NPP/Lite, Laurell Technologies Corporation, North Wales, PA, USA) at 2500–3000 rpm for 1.5 min. Some of the SiO_2 NP films were rinsed with DI water or NaOH solution (pH 10) for 10 s to deionize or re-ionize the NP surfaces, respectively.

PDMS (monodisperse PDMS or 1:1 mixture of the UV-curable PDMS precursors A and B) and PPC were dissolved in toluene and chloroform at a concentration of 4 wt%, respectively. Polymer layers of the desired thicknesses were coated on top of the SiO_2 NP films by spin coating the polymer solutions at 4000–5000 rpm for 30 s. PDMS was infiltrated into the interstices of the SiO_2 NPs via CaRI during/after spin coating, forming PDMS-infiltrated SiO_2 NP films. Unless otherwise noted, the monodisperse PDMS was used in this study. The UV-curable PDMS-infiltrated SiO_2 NP film was exposed to UV (illuminance ≈100 mW cm^{-2}, wavelength = 365 nm) for 30 s and aged for 24 h, to fully cure the PDMS. This film was used to obtain an SEM image of a PDMS-infiltrated SiO_2 NP film (Figure S1, Supporting Information) rather than to demonstrate the separation of polymer because uncured PDMS may contaminate the SEM chamber under vacuum. The bilayer film consisting of the PPC layer atop the SiO_2 NP film was heated in an oven (Model 20 Lab Oven, Quincy Lab, Inc., South Beloit, IL, USA) at 80 °C for 3 h to induce infiltration of PPC into the interstices of the NP packing via CaRI.

Film Characterization: The surface chemistry of the SiO_2 NP films was characterized by EDS analysis using an EDS detector (EDAX, AMETEK, Inc., Berwyn, PA, USA) mounted on a scanning electron microscope (SEM) (Quanta 600 FEG ESEM, FEI Company, Hillsboro, OR, USA). Prior to analysis, the films were coated with 4 nm Ir layers using a sputter coater (Q150TES, Quorum Technologies Ltd., Lewes, UK) to prevent possible charging. After focusing the films at a 5 kV electron beam voltage in the SEM, EDS signals were detected for 1 min. The analysis was performed using the TEAM EDS Analysis System (EDAX, Mahwah, NJ, USA). The microstructure of the UV-cured PDMS-infiltrated SiO_2 NP film was captured using a high-resolution SEM (JSM-7500F, JEOL Ltd., Tokyo, Japan) under

conditions of 5 kV electron beam voltage and 20 µA emission current. The film was coated with a 4 nm Ir layer prior to analysis as well.

The thickness and refractive index of films were determined using a spectroscopic ellipsometer (SE-2000, Semilab, Budapest, Hungary). The ellipsometer measured the amplitude ratio (Ψ) and the phase difference (Δ) of the complex reflection coefficients of light polarized parallel and perpendicular to the plane of incidence. The measurements were carried out at 75° of incidence angle in the photon energy range of 1.3–4.5 eV, and the measured optical data were analyzed by the SEA software to extract the thicknesses and refractive indices. Each transparent layer was modeled as a Cauchy layer, and the refractive index was represented by $n = A + B/\lambda^2 + C/\lambda^4$, where A, B, and C are optical constants and λ is the wavelength of light. Modeling was performed with a small mean square error (<5). The RH of the air surrounding the films was controlled using a humidity chamber (operated by a mass flow controller to ensure the ratio of dry and wet air inlet) compatible with the ellipsometer. For measurements in increased RH environments, the initial spectra were recorded at 40% RH, which was followed by an increase to a set RH value which was then kept constant in time.

Environmental ellipsometric porosimetry was carried out in the same humidity chamber by recording ellipsometric spectra stepwise at increasing/decreasing RH (in the RH range between 2%–100%-2%). Lorentz-Lorenz effective medium approximation (EMA) was used to model the refractive index of the SiO_2 NP packings partially filled with air and adsorptive (water) molecules to obtain the volume adsorbed/desorbed isotherms from the fitted refractive index values.[53] Porosity was calculated using the Lorentz-Lorenz EMA for the water-filled SiO_2 NP packings at RH = 100%, and the pore size distribution was obtained via the modified Kelvin equation.[53,54]

An upright optical microscope (Euromex, Arnhem, Netherlands) mounted with a CCD camera (MU800, AmScope, Irvine, CA, USA) was used in the reflection mode to observe microscopic changes in the PDMS-infiltrated SiO_2 NP films underwater. A 5 uL water drop was placed onto the film using a micropipette (0.5–10 µL, Eppendorf, Hamburg, Germany), and images were taken of the rim of the water drop to highlight the difference between the presence and absence of water. Contact angles were determined using a goniometer (Attension, Biolin Scientific, Gothenburg, Sweden).

Collection and Reuse of the Expelled PDMS Under High RH Using Depleted Elastomers: The 1:1 mixture of the UV-curable PDMS precursors A and B was degassed using a vacuum degasser. The mixture was then poured onto a Petri dish and exposed to UV (illuminance ≈100 mW cm^{-2}, wavelength = 365 nm) for 30 s and aged for 24 h, to fully cure the PDMS. The cured elastomer was cleaved into ≈1.5 × 1.5 cm^2 pieces and left in a toluene bath for 5 days, replacing the toluene used daily. Uncrosslinked chains were leached out using toluene, resulting in a depleted elastomer.[55] The depleted elastomers were stored in ethanol for 24 h, followed by 24 h in DI water to remove residual solvents. The PDMS-infiltrated SiO_2 NP (unionized) film, on which the depleted elastomer was in contact, was exposed to high humidity (RH ≈100%) for 10 min, and the expelled PDMS was collected into the elastomer. After repeating the collection from three different films, the PDMS loaded in the elastomer could be reused to fabricate a new PDMS-infiltrated SiO_2 NP film by contacting the elastomer with a new SiO_2 NP film for 1 min at RH ≈10% via leaching-enabled CaRI; the mobile PDMS chains infiltrate into the interstitial voids.[26]

Supporting Information

Supporting Information is available from the Wiley Online Library or from the author.

Acknowledgements

This work was supported by Penn MRSEC (NSF DMR-1720530). M.F. acknowledges funding from a UCL Chemical Engineering Impact Ph.D. studentship sponsored by Semilab.

Conflict of Interest

The authors declare no conflict of interest.

Data Availability Statement

The data that support the findings of this study are available from the corresponding author upon reasonable request.

Keywords

composite recycling, capillary condensation, polymer nanocomposites, porous materials

Received: March 29, 2023
Revised: May 9, 2023
Published online: June 1, 2023

[1] A. Sellinger, P. M. Weiss, A. Nguyen, Y. Lu, R. A. Assink, W. Gong, C. J. Brinker, *Nature* **1998**, *394*, 256.
[2] E. Munch, M. E. Lanuney, D. H. Alsem, E. Saiz, A. P. Tomsia, R. O. Ritchie, *Science* **2008**, *322*, 1516.
[3] L. J. Bonderer, A. R. Studart, L. J. Gauckler, *Science* **2008**, *319*, 1069.
[4] B. Yeom, T. Sain, N. Lacevic, D. Bukharina, S. H. Cha, A. M. Waas, E. M. Arruda, N. A. Kotov, *Nature* **2017**, *543*, 95.
[5] H. Zhao, S. Liu, Y. Wei, Y. Yue, M. Gao, Y. Li, X. Zeng, X. Deng, N. A. Kotov, L. Guo, L. Jiang, *Science* **2022**, *375*, 551.
[6] Y. Deng, J. Chen, C. Chang, K. Liao, K. Tung, W. E. Price, Y. Yamauchi, K. C. W. Wu, *Angew. Chem., Int. Ed.* **2016**, *128*, 12985.
[7] F. Ding, J. Liu, S. Zeng, Y. Xia, K. M. Wells, M.-P. Nieh, L. Sun, *Sci. Adv.* **2017**, *3*, e1701212.
[8] Z. Gemici, P. I. Schwachulla, E. H. Williamson, M. F. Rubner, R. E. Cohen, *Nano Lett.*. **2009**, *9*, 1064.
[9] B. Q. Kim, Y. Qiang, K. T. Turner, S. Q. Choi, D. Lee, *Adv. Mater. Interfaces* **2021**, *8*, 2001421.
[10] C. Dang, J. Lee, C. Breen, J. S. Steckel, S. Coe-Sullivan, A. Nurmikko, *Nat. Nanotechnol.* **2012**, *7*, 335.
[11] J. Lee, S. Kim, J. Lee, D. Yang, B. C. Park, S. Ryu, I. Park, *Nanoscale* **2014**, *6*, 11932.
[12] A. S. Pawbake, R. G. Waykar, D. J. Late, S. R. Jadkar, *ACS Appl. Mater. Interfaces* **2016**, *8*, 3359.
[13] D. W. Wang, F. Li, J. Zhao, W. Ren, Z. G. Chen, J. Tan, Z. S. Wu, I. Gentle, G. Q. Lu, H. M. Cheng, *ACS Nano* **2009**, *3*, 1745.
[14] E. Bakangura, L. Wu, L. Ge, Z. Yang, T. Xu, *Prog. Polym. Sci.* **2016**, *57*, 103.
[15] Q. Chen, S. Gong, J. Moll, D. Zhao, S. K. Kumar, R. H. Colby, *ACS Macro Lett.*. **2015**, *4*, 398.
[16] Y. Qiang, K. T. Turner, D. Lee, *Macromolecules* **2023**, *56*, 122.
[17] Y. Qiang, S. S. Pande, D. Lee, K. T. Turner, *ACS Nano* **2022**, *16*, 6372.
[18] Y. Jiang, J. L. Hor, D. Lee, K. T. Turner, *ACS Appl. Mater. Interfaces* **2018**, *10*, 44011.
[19] R. B. Venkatesh, N. Manohar, Y. Qiang, H. Wang, H. H. Tran, B. Q. Kim, A. Neuman, T. Ren, Z. Fakhraai, R. A. Riggleman, K. J. Stebe, K. Turner, D. Lee, *Annu. Rev. Chem. Biomol. Eng.* **2021**, *12*, 411.
[20] C. Harito, D. v. Bavykin, B. Yuliarto, H. K. Dipojono, F. C. Walsh, *Nanoscale* **2019**, *11*, 4653.
[21] H. Zhu, Y. Li, Z. Fang, J. Xu, F. Cao, J. Wan, C. Preston, B. Yang, L. Hu, *ACS Nano* **2014**, *8*, 3606.
[22] R. Hoffmann, V. Baric, H. Naatz, S. O. Schopf, L. Mädler, A. Hartwig, *ACS Appl. Nano Mater.*. **2019**, *2*, 2273.
[23] H. Zhang, M. Popp, A. Hartwig, L. Mädler, *Nanoscale* **2012**, *4*, 2326.

[24] Y. R. Huang, Y. Jiang, J. L. Hor, R. Gupta, L. Zhang, K. J. Stebe, G. Feng, K. T. Turner, D. Lee, *Nanoscale* **2015**, *7*, 798.
[25] J. L. Hor, Y. Jiang, D. J. Ring, R. A. Riggleman, K. T. Turner, D. Lee, *ACS Nano* **2017**, *11*, 3229.
[26] R. B. Venkatesh, S. H. Han, D. Lee, *Nanoscale Horiz.*. **2019**, *4*, 933.
[27] N. Manohar, K. J. Stebe, D. Lee, *ACS Macro Lett.* **2017**, *6*, 1104.
[28] M. Prinçaud, C. Aymonier, A. Loppinet-Serani, N. Perry, G. Sonnemann, *ACS Sustainable Chem. Eng.* **2014**, *2*, 1498.
[29] J. Jiang, G. Deng, X. Chen, X. Gao, Q. Guo, C. Xu, L. Zhou, *Compos. Sci. Technol.* **2017**, *151*, 243.
[30] J. M. Garcia, M. L. Robertson, *Science* **2017**, *358*, 870.
[31] Y. Yang, R. Boom, B. Irion, D. J. van Heerden, P. Kuiper, H. de Wit, *Chem. Eng. Process.* **2012**, *51*, 53.
[32] J. Pourchez, C. Chivas-Joly, C. Longuet, L. Leclerc, G. Sarry, J. M. Lopez-Cuesta, *Environ. Sci.: Nano* **2018**, *5*, 1951.
[33] F. Restagno, L. Bocquet, T. Biben, *Phys. Rev. Lett.* **2000**, *84*, 2433.
[34] T. Hiratsuka, H. Tanaka, M. T. Miyahara, *J. Chem. Phys.* **2016**, *144*, 164705.
[35] C. Desgranges, J. Delhommelle, *Langmuir* **2019**, *35*, 15401.
[36] K. Xing, S. Chatterjee, T. Saito, C. Gainaru, A. P. Sokolov, *Macromolecules* **2016**, *49*, 3138.
[37] B. P. Binks, J. H. Clint, *Langmuir* **2002**, *18*, 1270.
[38] G. C. Randall, P. S. Doyle, *Proc. Natl. Acad. Sci. USA* **2005**, *102*, 10813.
[39] P. Bian, Y. Wang, T. J. McCarthy, *Macromol. Rapid Commun.* **2021**, *42*, 2000682.
[40] N. J. Alvarez, L. M. Walker, S. L. Anna, *J. Colloid Interface Sci.* **2009**, *333*, 557.
[41] B. K. Primkulov, J. Y. Y. Chui, A. A. Pahlavan, C. W. Macminn, R. Juanes, *Phys. Rev. Lett.* **2020**, *125*, 174503.
[42] J. Andre, K. Okumura, *Langmuir* **2020**, *36*, 10952.
[43] O. McRae, T. S. Ramakrishnan, J. C. Bird, *J. Colloid Interface Sci.* **2022**, *608*, 1919.
[44] M. Kosmulski, *Chemical Properties of Material Surfaces*, Vol. *102*, (Ed: T. A. Hubbard), Marcel Dekker, New York, NY, **2001**.
[45] L. T. Zhuravlev, *Colloids Surf A Physicochem Eng Asp* **2000**, *173*, 1.
[46] F. S. Emami, V. Puddu, R. J. Berry, V. Varshney, S. V. Patwardhan, C. C. Perry, H. Heinz, *Chem. Mater.* **2014**, *26*, 2647.
[47] J. M. Rimsza, R. E. Jones, L. J. Criscenti, *J. Colloid Interface Sci.* **2018**, *516*, 128.
[48] R. K. Gupta, G. J. Dunderdale, M. W. England, A. Hozumi, *J. Mater. Chem. A* **2017**, *5*, 16025.
[49] J. Gu, L. Ji, P. Xiao, C. Zhang, J. Li, L. Yan, T. Chen, *ACS Appl. Mater. Interfaces* **2021**, *13*, 36679.
[50] Y. Qin, L. Chen, X. Wang, X. Zhao, F. Wang, *Carbohydr. Polym.* **2011**, *84*, 329.
[51] M. C. Gurau, S. M. Lim, E. T. Castellana, F. Albertorio, S. Kataoka, P. S. Cremer, *J. Am. Chem. Soc.* **2004**, *126*, 10522.
[52] S. Prakash, E. Xi, A. J. Patel, *Proc. Natl. Acad. Sci. U. S. A.* **2016**, *113*, 5508.
[53] A. Alvarez-Fernandez, B. Reid, M. J. Fornerod, A. Taylor, G. Divitini, S. Guldin, *ACS Appl. Mater. Interfaces* **2020**, *12*, 5195.
[54] B. M. Baklanov, K. P. Mogilnikov, V. G. Polovinkin, F. N. Dultsev, *J. Vac. Sci. Technol., B: Microelectron. Nanometer Struct.–Process., Meas., Phenom.* **2000**, *18*, 1385.
[55] R. B. Venkatesh, D. Lee, *Macromolecules* **2022**, *55*, 8659.